



HAL
open science

As(V) sorption from aqueous solutions using quaternized algal/polyethyleneimine composite beads

Mohammed Hamza, Siming Lu, Khalid A.M. Salih, Hamed Mira, Abdelghaffar Dhmees, Toyohisa Fujita, Yuezhou Wei, Vincent Thierry, Eric Guibal

► To cite this version:

Mohammed Hamza, Siming Lu, Khalid A.M. Salih, Hamed Mira, Abdelghaffar Dhmees, et al.. As(V) sorption from aqueous solutions using quaternized algal/polyethyleneimine composite beads. *Science of the Total Environment*, 2020, 719, pp.137396. 10.1016/j.scitotenv.2020.137396 . hal-02489375

HAL Id: hal-02489375

<https://imt-mines-ales.hal.science/hal-02489375v1>

Submitted on 5 Mar 2020

HAL is a multi-disciplinary open access archive for the deposit and dissemination of scientific research documents, whether they are published or not. The documents may come from teaching and research institutions in France or abroad, or from public or private research centers.

L'archive ouverte pluridisciplinaire **HAL**, est destinée au dépôt et à la diffusion de documents scientifiques de niveau recherche, publiés ou non, émanant des établissements d'enseignement et de recherche français ou étrangers, des laboratoires publics ou privés.

As(V) sorption from aqueous solutions using quaternized algal/polyethyleneimine composite beads

Mohammed F. Hamza^{a,b}, Siming Lu^a, Khalid A.M. Salih^a, Hamed Mira^b, Abdelghaffar S. Dhmees^c, Toyohisa Fujita^a, Yuezhou Wei^{a,d,**}, Thierry Vincent^e, Eric Guibal^{e,*}

^a Guangxi Key Laboratory of Processing for Non-ferrous Metals and Featured Materials, School of Resources, Environment and Materials, Guangxi University, Nanning 530004, China

^b Nuclear Materials Authority, POB 530, El-Maadi, Cairo, Egypt

^c Egyptian Petroleum Research Institute, El Zohour Region, Nasr City, Cairo 11727, Egypt

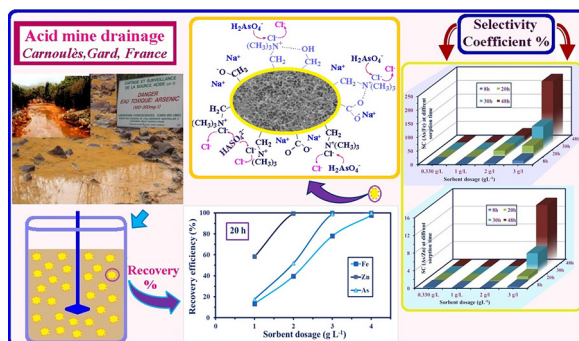
^d Shanghai Jiao Tong University, Shanghai, China

^e Polymers Composites and Hybrids (PCH) IMT – Mines Ales, F-30319 Alès cedex, France

HIGHLIGHTS

- As(V) sorption on algal/PEI beads is strongly improved by bead quaternization.
- At pH close to 7, sorption capacity reaches up to 1.34 mmol As g⁻¹ (100 mg As g⁻¹).
- Fast uptake kinetics is fitted by the pseudo-first order rate equation.
- As(V) is desorbed with acidic CaCl₂ solutions (with good sorbent recycling).
- The sorbent is highly efficient as a polishing treatment for acid mine drainage.

GRAPHICAL ABSTRACT



ABSTRACT

Composite beads (APEI*), obtained by the controlled interaction of algal biomass with PEI, followed by ionotropic gelation and crosslinking processes using CaCl₂/glutaraldehyde solution, constitute efficient supports for metal binding. The quaternization of algal/PEI beads (Q-APEI*) significantly increases the sorption properties of the composite beads (APEI*) for As(V). The materials are characterized by SEM/EDX, TGA, BET, elemental analysis, FTIR, XPS, and titration. The sorption of As(V) is studied in function of pH while sorption mechanism is discussed in function of metal speciation and surface characteristics of the sorbent. Optimum sorption occurs at pH close to 7. Fast uptake kinetics, correlated to textural properties are successfully fitted by pseudo-first order rate equation and the Crank equation (for resistance to intraparticle diffusion); equilibrium is reached with 45–60 min. The Langmuir equation finely fits sorption isotherms; maximum sorption capacity reaches 1.34 mmol As g⁻¹. Arsenic can be completely eluted using 0.5 M CaCl₂/0.5 M HCl solutions; the sorbent maintains high sorption and desorption efficiencies for a minimum of 5 cycles. The sorbent is tested for the removal of As(V) from mining effluents containing high concentration of iron and traces of zinc. At pH 3, the sorbent shows remarkable selectivity for As(V) over Fe. After controlling the initial pH to 5, a sorbent dosage of 2 g L⁻¹ is sufficient for achieving the complete recovery of As(V) from mining effluent (corresponding to initial concentration of 1.295 mmol As L⁻¹).

Keywords:

Quaternization
Algal/PEI composite beads
Arsenic sorption
Sorption isotherm and uptake kinetics
Desorption and recycling
Treatment of mining effluent

* Corresponding author.

** Correspondence to: Yuezhou Wei, Guangxi Key Laboratory of Processing for Non-ferrous Metals and Featured Materials, School of Resources, Environment and Materials, Guangxi University, Nanning 530004, China

E-mail addresses: fujitatoyohisa@gxu.edu.cn (T. Fujita), yzwei@gxu.edu.cn (Y. Wei), thierry.vincent@mines-ales.fr (T. Vincent), eric.guibal@mines-ales.fr (E. Guibal).

1. Introduction

Arsenic is an acute and serious threat in many countries because of anthropogenic contamination (associated with mining exploitation) but also of naturogenic sources (natural drainage of soil and ores with high As content) (Drahota et al., 2012; Ng et al., 2003). In such places, the exposure of population to contaminated water (drinking water) or food (plant irrigation, fishing and farming) may cause drastic health problems associated with As accumulation in the organisms (Halder et al., 2014; Miller et al., 2004): skin lesion, bladder, kidney and lung cancers but also diseases such as diabetes, blood pressure and reproductive disorders (Phan et al., 2010). Regulations on the level of arsenic in drinking water, irrigation water or animal farming are thus becoming very strict. For example, US EPA is recommending levels lower than $10 \mu\text{g L}^{-1}$ for drinking water (USEPA, 2012), while FAO requests arsenic being lower than $100 \mu\text{g L}^{-1}$ in water for irrigation purpose (Jeong et al., 2016). The toxicity of arsenic depends on its speciation in water and food.

The removal of arsenic is thus a critical topic in many countries that can explain the numerous research projects for designing new treatment processes. Coagulation/flocculation, eventually coupled with membrane processes, has been investigated (Kumar and Quaff, 2019; Oehmen et al., 2011), precipitation was also used for removing arsenic from leaching liquors (Li et al., 2019); these processes can be mediated by biological activity (Farasin et al., 2015; Zacarias-Estrada et al., 2019). However, the processes the most frequently reported are associated with sorption on a wide variety of supports (Asere et al., 2019). Activated carbon is a sorbent widely investigated for water decontamination, including for the recovery of arsenic, such as Japanese oak wood-based biochar (Niazi et al., 2018), especially after impregnation with metal ions and iron (Agrawal et al., 2016; Deliyanni et al., 2015; Sigrift et al., 2011; Thi Hanh et al., 2019). Natural and functionalized clays have retained attention for the last decade (Barakan and Aghazadeh, 2019; Foroutan et al., 2019; Tiwari and Lee, 2012; Tuchowska et al., 2019). Iron oxide or hydroxide and other metal oxides were also used for developing simple or sophisticated sorbents consisting of their immobilization in porous organic and inorganic matrices (Chaudhry et al., 2017; Dong et al., 2019; Elwakeel and Guibal, 2015; Haron et al., 1999; Padungthong et al., 2015; Wei et al., 2019b; Yin et al., 2019; Yousif et al., 2016). The affinity of arsenic for molybdate was used for recovering the metalloid on molybdate-impregnated chitosan beads (Dambies et al., 2002). Ion-exchange resins (Jose Alguacil and Escudero, 2018) and impregnated resins (Ciopec et al., 2014) have also been carried out for the treatment of As-containing solutions. Biosorbents opened also promising perspectives for As(III) and As(V) sorption; agriculture wastes can be used as produced or chemically modified (Shakoor et al., 2018). Biopolymers such as alginate or starch have also retained attention for stabilizing or encapsulating metal oxide (He et al., 2020; Yan et al., 2019).

Recently, a new generation of composite materials (APEI*) based on the interaction of algal biomass and polyethyleneimine (PEI) has been designed (Wang et al., 2019). The process is based on the one-pot partial extraction of alginate from brown-algae and the interaction of extracted alginate with amine groups from PEI, followed by the simultaneous glutaraldehyde crosslinking of amine groups of PEI and ionotropic gelation of carboxylate groups with CaCl_2 . This composite sorbent bears multifunctional groups (amine and carboxylic groups). In order to enhance sorption properties, the sorbent can be functionalized by grafting specific reactive groups such as amidoxime (Wei et al., 2019a).

The quaternization of APEI* (to synthesize Q-APEI*) can be performed by reaction of glycidyltrimethylammonium chloride with the amine groups hold on APEI*. This quaternization is expected to increase the density of protonated amine groups on a larger range of pH. This functionalization is supposed to enhance the ability of the sorbent for binding anions. This is especially interesting for the sorption of As(V) anions, which are predominant in solution at pH higher than

2.5–3. The functionalized sorbent is characterized physically and chemically using a wide range of analytical tools (detailed discussion appearing in the additional material section, AMS), before investigating As(V) sorption properties through the study of pH effect, uptake kinetics and sorption isotherms. The desorption of arsenic and the recycling of the sorbent are investigated through five successive cycles. In the last part of the work the sorbent is tested for the treatment of acid mine drainage.

2. Materials and methods

2.1. Materials

Laminaria digitata, brown algae, was supplied by Setalg (Pleubian, France). Branched PEI (50%, w/w in water) and glutaraldehyde were purchased from Sigma-Aldrich (Taufkirchen, Germany). Sodium carbonate and calcium chloride were supplied by Chem-Lab NV (Zedelgem, Belgium). Sodium arsenate (used as the source of arsenic for synthetic solutions) was purchased from Johnson Fine Chemicals (Bangalore, India). Glycidyltrimethylammonium chloride ($\geq 95\%$) and ethylene glycol diglycidyl ether as crosslinking agent were supplied by Shanghai Maklin Biochemical Co., Ltd. (Shanghai, China). All other reagents are Prolabo products and used as received.

As(V) solution was collected from the tailing dam of an abandoned polymetallic mine at Carnoulès (Gard, France).

2.2. Synthesis of sorbent

2.2.1. APEI* beads

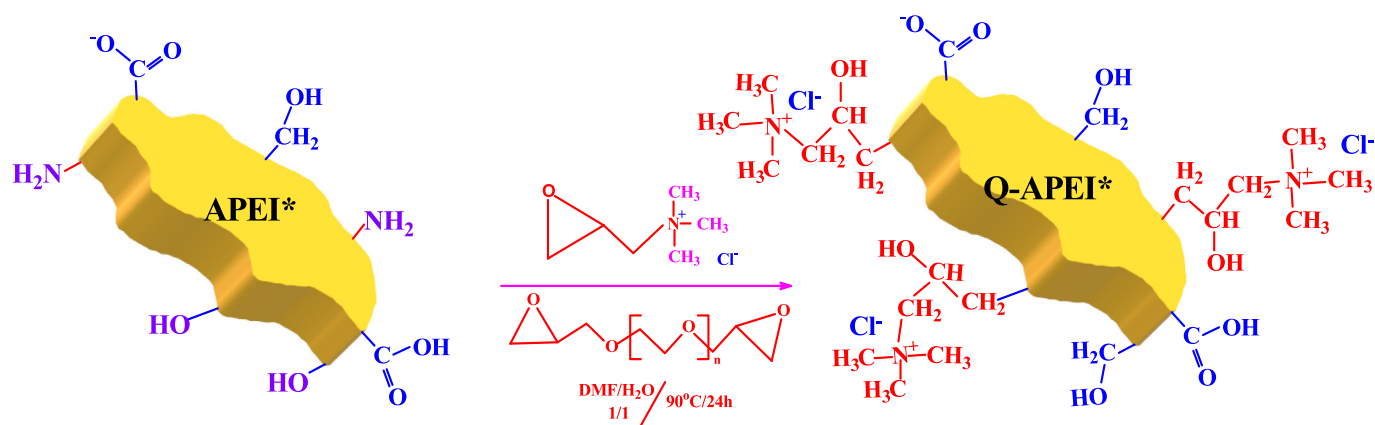
Twenty g of *L. digitata* were mixed with 600 mL of 1% Na_2CO_3 (w/w) and maintained at 50°C for 24 h. This step induces the partial extraction of alginate contained in the wall of algal biomass (Wang et al., 2018). Thereafter, 5 mL of PEI solution (50%, w/w) were added to the mixture and the suspension was dropped into 1 L of CaCl_2/GA solution (1% CaCl_2 , w/w; 5 mL GA, 50% w/w) for manufacturing APEI* beads. Calcium chloride contributes to the ionotropic gelation of alginate (carboxylate groups) while glutaraldehyde crosslinks PEI (amine groups). The beads (APEI*) are washed thoroughly and freeze-dried (-52°C , 0.1 mbar) for two days.

2.2.2. Quaternization procedure – Q-APEI* beads (Scheme 1)

Three g (dry weight) of poly(ethyleneglycol) diglycidyl ether (used for improving the crosslinking of the beads; enhanced stability of the beads for successive contacts with acid and base solutions) was dissolved into 100 mL DMF:H₂O (1:1 v/v) solution. Five g (dry weight) of beads were dropped into the solution in the presence of 10 g of glycidyltrimethyl ammonium chloride (quaternizing agent). The mixture was refluxed at 90°C under gentle agitation (95 rpm) for 24 h. Finally, the quaternized beads (Q-APEI*) were filtered off, rinsed with hot water for removing unreacted materials and then with methanol before being dried under vacuum for 10 h at 50°C .

2.3. Characterization of materials

Chemical composition of the beads before and after modification were analyzed using FT-IR spectrometry (Shimadzu, Tokyo, Japan), and XPS analysis (Thermo Fischer Scientific, Inc., Waltham, MA, USA). The surface characteristics were investigated using scanning electron microscopy SEM (Thermo Fisher Scientific, Eindhoven, The Netherlands) while the chemical composition of the surface was analyzed using EDX analysis (integrated to Phenom ProX SEM). The surface area and the porosity of the sorbents (raw material and modified QA) were performed using Micromeritics TriStar II analyzer (Norcross, GA, USA). Elemental analysis was carried out on a Vario EL Cube (Elementar Analysensysteme GmbH, Langenselbold, Germany). Thermal decomposition of the beads was carried out using TG-DTA (Netzsch STA 449 F3



Scheme 1. Reaction pathway for the functionalization of APEI* → Q-APEI*.

Jupiter, NETZSCH-Gerätebau GmbH, Selb, Germany). The pH_{PZC} was obtained by the pH drift method. Experimental procedures were more detailed in previous work (Lu et al., 2019). More details may be also found in the Additional Material Section (AMS).

2.4. Sorption studies

Arsenic sorption properties of APEI* and Q-APEI* were compared using batch processing. A fixed volume of solution (V , L), containing a known concentration of arsenic (C_0 , mmol As L^{-1}) at fixed initial pH (pH_0) was mixed with a fixed amount of sorbent (m , g; giving a sorbent dosage, SD: m/V , g L^{-1}), at room temperature (i.e., T : $22 (\pm 2) ^\circ\text{C}$). The suspension was maintained under agitation (v : $165 (\pm 5)$ rpm) for fixed contact time. The final pH (pH_{eq}) was measured and the residual concentration (C_{eq} , mmol As L^{-1}) was determined after filtration ($1.2 \mu\text{m}$ pore size filter membrane) by ICP-AES (ICPS-7510 Shimadzu, Japan); the detection limit is close to $0.005 \text{ mg As L}^{-1}$. The sorption capacity (q_{eq} , mmol As g^{-1}) was determined by the mass balance equation: $q_{\text{eq}} = (C_0 - C_{\text{eq}}) \times V/m$.

As-loaded sorbent was desorbed using $0.5 \text{ M CaCl}_2/0.5 \text{ M HCl}$ solution in the batch mode. The efficiency of desorption was calculated by the mass balance between the amount of As sorbed and the amount of As released in the eluate. After the desorption step, collected beads were abundantly rinsed with demineralized water for re-use.

The modeling of sorption performances was performed using conventional equations (uptake kinetics, sorption isotherms and desorption kinetics), which are summarized in Tables AM 1–3. The models were fitted using non-linear regression analysis (Mathematica® facilities) and fitted values were compared with experimental data for calculating determination coefficients.

The experimental conditions are systematically reported in the caption of the figures. The reproducibility of sorption performance is confirmed by repeated experiments (1st Series and 2nd Series), appearing on Figures.

2.5. Application on real effluent

Application of Q-APEI* for the treatment of real effluents (acid mine drainage, AMD) was investigated using samples collected at the outlet of the tailing dam of a polymetallic abandoned mine located at Carnoulès (France). The exposure of sulfur-rich residues to air and rain causes important release of contaminated acid effluents containing concentrations as high as 200 mg As L^{-1} (i.e., $2.67 \text{ mmol As L}^{-1}$) and iron (higher than 1.3 g Fe L^{-1} ; $23.3 \text{ mmol Fe L}^{-1}$) in addition to many other inorganic contaminants (Farasin et al., 2015). The effect of pH on the sorption of As, Fe and Zn (sorption capacity and removal efficiency) was investigated at different values; the precipitation of selected metals at fixed pH values was analyzed. After adjusting the pH

to target value, the solution was filtrated and the residual concentrations of As(V) and other co-existing elements were analyzed. The sorption tests were performed on filtrated solutions to isolate sorption from precipitation effect. The effect of sorbent dosage (from 0.33 to 3 g L^{-1}) was finally tested on AMD at $\text{pH}_0 5$ (pH_{eq} : 6.3 – 5.9).

3. Results and discussion

3.1. Characterization of sorbent

3.1.1. Physical characterization

The size of APEI* is measured by scaled optical photograph (Figure AM1, see Additional Material Section): with average diameter close to $2.19 \pm 0.2 \text{ mm}$; this size is not significantly affected by the functionalization of raw beads. The textural characteristics of Q-APEI* (determined using BET analysis, Figure AM2) show that the sorbent is porous: specific surface is close to $28.6 \text{ m}^2 \text{ g}^{-1}$; while mesoporous volume is around $0.035 \text{ cm}^3 \text{ g}^{-1}$, with diameter below 20 nm , while the average pore size is close to 2 nm .

3.1.2. Chemical characterization

3.1.2.1. Elemental analysis. The elemental analysis is summarized in Table 1. The quaternization of APEI* increases the fraction of N element in the sorbent: molar content increases from $4.92 \text{ mmol N g}^{-1}$ to $8.00 \text{ mmol N g}^{-1}$. It is difficult to evaluate the yield of substitution since PEI bears different types of amine groups: primary/secondary/tertiary amines are distributed according the proportions 1:2:1 in branched PEI. Their interactions with carboxylate groups (direct ionic binding) and with glutaraldehyde (crosslinking) affect the availability of amine groups for functionalization. However, nitrogen content increases by 62%: the quaternization of amine groups is highly efficient.

3.1.2.2. FTIR spectroscopy. FTIR analysis confirms the chemical modification of APEI* beads (Figure AM3 for 1800 – 400 cm^{-1} wavenumber range, and Table AM4, detailed assignment of peaks). The quaternization of raw beads is characterized by:

- (a) appearance of a peak around 1480 cm^{-1} , assigned to quaternary ammonium,

Table 1
Elemental analysis of sorbents.

Sorbent	N [%]	N [mmol g^{-1}]	C [%]	H [%]	O [%]	S [%]	Cl [%]
APEI*	6.89	4.92	54.97	6.93	23.99	0.22	0.78
Q-APEI*	11.21	8.00	55.05	7.05	24.68	0.05	1.56

- (b) widening of the band at 1613 cm^{-1} (N—H bending and carboxylic acid salt), attributed to the overlapping of a signal representative of imino group (in open chain) and to carboxylate groups,
- (c) appearance of peaks in the range $1030\text{--}1060\text{ cm}^{-1}$, associated with C—N and C—O stretching vibrations.
- (d) appearance of a peak at 963 cm^{-1} , attributed to C—N stretching vibration.

After As(V) sorption the FTIR spectrum is characterized by the appearance of a peak at 1740 cm^{-1} ; this is usually assigned to C=O from carboxylic groups. However, in the present case, this probably means that the electronic environment of amine groups (usually found at $1620\text{--}1650\text{ cm}^{-1}$) is affected by As(V) binding. In addition, the intensity of the peak at 1410 cm^{-1} strongly decreases; this peak is usually assigned to carboxylic acid salt. The peak at 613 cm^{-1} is shifted to 619 cm^{-1} with a significant increase of the intensity after As(V) uptake. It is noteworthy that these peaks almost disappear after arsenic desorption: the FTIR spectrum is very close to that of Q-APEI* beads before sorption. The sorbent is efficiently regenerated. After five cycles of sorption and desorption, the FTIR spectrum is also very close to the spectrum of the original functionalized beads. The most significant difference appears with the peak at 1734 cm^{-1} , which only appeared for As(V)-loaded Q-APEI*.

3.1.2.3. XPS spectroscopy. Fig. 1 shows the survey XPS spectra of APEI*, Q-APEI* (before and after As(V) sorption). The quaternization is mainly characterized by the appearance of the Cl 2p signal, which corresponds to the counter-anion of quaternary ammonium group on the sorbent. The presence of S element is associated to the presence of fucoidan in the wall of brown algae. On the survey curve, the functionalization only changes the relative fraction of the elements. The binding of As (V) is ascertained by the appearance of the signals for As 3d and As 3p. The high-resolution spectra of selected bands (and their deconvolution) are shown in Figure AM4; the binding energies (BEs) and the atomic fraction of the different compounds are reported in Table AM5. The functionalization of APEI* is demonstrated by the strong variations observed in the environment of N signals. The deconvolution of N 1s signal shows that the quaternization drastically increases, as expected, the intensity of the signal associated with tertiary amine group. In addition, the asymmetry of the C 1s signal changes with the evolution of the material: actually after As(V) sorption the material approaches the profile of APEI* spectrum contrary to Q-APEI*.

(O, =N) decreases with functionalization but is restored with As (V) sorption: this confirms that the sorption of As(V) affects the environment of C=N groups. The As $3d_{3/2}$ band does not show deconvolution peaks: this means that As is only bound through a single and specific bonding, probable binding of anionic As(V) species to protonated amine groups (quaternary ammonium) (see below expected binding mechanism). Indeed, FTIR and XPS analyses showed that the environment of N groups is affected by metalloid binding. The analysis of deconvoluted peaks for Cl 2p signal indicates the coexistence of different Cl groups (depending on the type of N groups; i.e., primary/secondary and quaternary ammonium groups) on Q-APEI*, while after As (V) sorption a part of these chloride anions is exchanged with anionic As(V) species.

3.1.2.4. TGA analysis. The thermal degradation of APEI* and Q-APEI* materials are reported in Figure AM5. The two materials are characterized by different profiles. Both show a relatively similar weight loss (14–17%) associated with release of water bound at the surface or in the porous network, at low temperature (below $200\text{ }^\circ\text{C}$) (Dos Santos Araujo et al., 2019). When the temperature increases, the differences are more marked. APEI* shows a progressive weight loss between 200 and $700\text{ }^\circ\text{C}$; at $700\text{ }^\circ\text{C}$, the sorbent is completely degraded. This degradation takes place in two steps with the maximum degradation rates in dTGA detected at $245.3\text{ }^\circ\text{C}$ and $615.4\text{ }^\circ\text{C}$, respectively. The first part is associated with the depolymerization of the polymers (carbohydrates and PEI), the second step being assigned to the degradation of monomers (amine groups, etc.) and the decomposition of the char under air atmosphere. In the case of the thermochemical characterization of *Laminaria digitata*, two steps corresponding to the devolatilization (around $245\text{ }^\circ\text{C}$) and the char formation (around $545\text{ }^\circ\text{C}$) were identified (Membere and Sails, 2018). Above, $600\text{ }^\circ\text{C}$, the char progressively decomposed. With the incorporation of PEI, the first critical temperature is not influenced by the quaternization, while for the second step, the limit temperature is increased from $545\text{ }^\circ\text{C}$ to $615\text{ }^\circ\text{C}$. In the case of the thermal degradation of functionalized PEI microgels, the onset degradation of PEI was observed at $180\text{ }^\circ\text{C}$ and increased with chemical modification (up to $249\text{ }^\circ\text{C}$, depending on the substituent) and continued up to $416\text{ }^\circ\text{C}$ for PEI microgels (up to $383\text{--}408\text{ }^\circ\text{C}$ for chemically modified gels). Some substituents increased the thermal stability of PEI microgels (for example, butyronitrile, ethylamine ethanol) while other (such as glycidol) tends to decrease the stability of the gel (Sahiner et al., 2015).

For Q-APEI*, two steps are also identified:

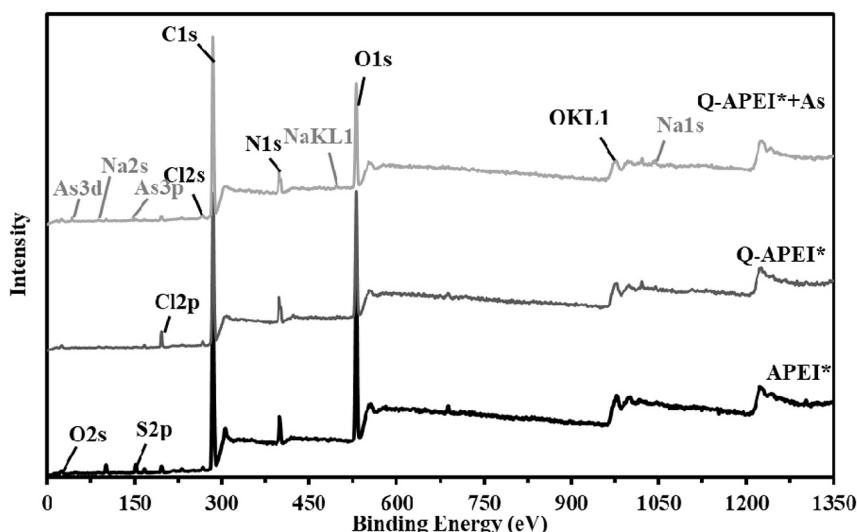


Fig. 1. XPS characterization of APEI*, Q-APEI* (before and after As(V) sorption) – Survey spectra.

- (a) between 200 and 350 °C (additional weight loss: $\approx 50\%$), associated with depolymerization and degradation of some reactive groups (probably grafted quaternary ammonium salts, (Xiao et al., 2018)); the maximum degradation rate is observed at 263.5 °C, and.
- (b) above 350 °C and up to 800 °C (additional weight loss: $\approx 20\%$), attributed to decomposition of additional reactive groups and degradation of polymer char (Liu et al., 2016). Several waves of lower intensity (in the dTGA spectrum) are identified.

In the case of PVA/PEI membranes, the thermal stability of the membrane was increased by the GA crosslinking and the increasing fraction of PEI in the composite (Xiao et al., 2018). This was explained by the formation of both H-bonds and supplementary chemical bonds.

Intermediary degradation is stronger for Q-APEI*, while a higher temperature is necessary for achieving its complete degradation (compared with APEI*).

3.1.2.5. pH_{PZC} . Hamza et al. (2020) reported the quaternization of another type of beads prepared by a procedure similar to the current process, except that alginate was added to the formulation. The pH_{PZC} of APEI* prepared with additional incorporation of alginate was reported close to 4.9 and increased to 6.7 after quaternization. Here, without addition of alginate, the pH_{PZC} values for APEI* and Q-APEI* are found close to 4.41 and 5.71, respectively (Figure AM6). Alginate (from algal biomass) is constituted of mannuronic acid (pK_a of carboxylic groups: 3.38) and guluronic acid (pK_a of carboxylic groups: 3.65), while PEI bears primary, secondary and tertiary amine groups (pK_a : 4.5, 6.7 and 11.6, respectively) (Hamza et al., 2020). These different reactive groups contribute to set the acid-base properties and surface charge of APEI*; the grafting of quaternary ammonium salt shifts the charge balance to higher pH values making the sorbent protonated under mild acidic conditions with possibility to attract anionic species, including As(V) anions.

3.2. Sorption properties

3.2.1. pH effect

Fig. 2a compares the effect of pH on the sorption of As(V) for APEI* and Q-APEI*. APEI* sorbent shows negligible sorption of As(V) (<0.021 mmol As g^{-1} ; i.e., 1.6 mg As g^{-1}), regardless of the equilibrium pH (in the range 2–9). Figure AM7a shows the speciation diagram of As(V) under the experimental conditions selected for the study of pH effect. Below pH 2.5, H_3AsO_4 is the predominant As(V) species. Between pH 2.5 and 7, anionic $H_2AsO_4^-$ species predominates while above pH 7 di-anionic $HA_2O_4^{2-}$ is the main As(V) species (at least below pH 10). The pH_{PZC} of APEI* being close to 4.41, As(V) should be adsorbed preferentially in the pH range 2.5–4.5 through binding of anionic species on protonated amine groups. However, the negligible sorption capacity tends to demonstrate that the protonated amine groups are not available for binding As(V) anions; probably because they are engaged in crosslinking with glutaraldehyde or interactions with carboxylate groups of alginate extracted from *L. digitata*. On the opposite hand, Q-APEI* remains protonated on a wider pH range (pH_{PZC} : 5.71); in addition, the grafting of quaternary ammonium salt brings strong reactive groups for the binding of anionic compounds such as $H_2AsO_4^-$. Fig. 2 shows that As(V) sorption is negligible up to pH 3.5 and strongly increases till reaching 6.8 (q_{eq} : 0.66 mmol As g^{-1}). Above pH 6.8, the sorption capacity progressively decreases due to the progressive deprotonation of reactive groups and the predominance of $HA_2O_4^{2-}$, which would require two quaternary ammonium groups for binding (see below expected binding scheme). It is noteworthy that even at pH 8.8 the sorption capacity remains relatively high (i.e., 0.25 mmol As g^{-1}). This residual sorption affinity appears difficult to explain

while considering both the As(V) speciation and the overall surface charge. In strongly alkaline solutions, the charge shielding effect of Na^+ ions on negatively charged nitrogen and oxygen (on hydroxyl and carboxylate groups) may contribute to As(V) binding (see below expected interaction scheme).

Figure AM8 shows the pH variation during As(V) sorption: the pH change does not exceed one pH unit. Below pH_{PZC} the equilibrium pH tends to increase; a reciprocal trend is observed above the pH_{PZC} ; at least for Q-APEI*. Indeed, for APEI* the pH variation is negligible in the second section of the curve. These pH variations are less marked than the pH changes observed during the determination of pH_{PZC} values by the pH-drift method.

Figure AM9 shows the \ln_{10} plot of the distribution ratio (D , q_{eq}/C_{eq} , $L g^{-1}$) vs. pH_{eq} . The slope of the curve is correlated to the ion-exchange stoichiometry between quaternary ammonium groups and As(V) anions. The slope is close to 1.19; this confirms that most of As(V) sorption occurs by binding one mono-anionic $H_2AsO_4^-$ onto one quaternary ammonium group.

3.2.2. Uptake kinetics

Under selected experimental conditions (i.e., C_0 : ≈ 0.7 mmol As L^{-1} ; pH_0 : 7; SD: 1 $g L^{-1}$), As(V) sorption on Q-APEI* is a fast phenomenon: the equilibrium is reached within 45 min. Sorption may be controlled by different mechanisms including mass-transfer steps (including resistance to bulk, film and/or intraparticle diffusion) and proper reaction rates (Tien, 1994). Sufficient agitation avoids the resistance to bulk diffusion and minimizes the effect of resistance to film diffusion. In order to evaluate the relative contributions of these different mechanisms, the kinetic profiles are fitted with the pseudo-first order rate equation (PFORE, Fig. 2b), the pseudo-second order rate equation (PSORE, Figure AM10) (Ho and McKay, 1999) and the resistance to intraparticle diffusion (RIDE, Crank equation, Figure AM11) (Crank, 1975). Table 2 reports the parameters of the models (including the determination coefficients of relevant fits). The PFORE fits much better experimental data than the two other models: the calculated values for q_{eq} are closer to experimental values than with the PSORE: the fitted PSORE curves tend to overestimate the equilibrium concentration of As(V) in the solution. The RIDE gives R^2 values comparable with those of PSORE. The PFORE model is usually associated with physical-type interactions; this is consistent with the ion-exchange mechanism. The calculated value of the effective diffusivity in the sorbent is varying between 2.72×10^{-8} $m^2 min^{-1}$ and 4.50×10^{-8} $m^2 min^{-1}$ for the two series; this shows a certain variability in the kinetic profiles probably associated to differences in the porosity of the beads. It is noteworthy that the self-diffusivity of As(V) in water is close to 5.43×10^{-8} $m^2 min^{-1}$ (Marcus, 1997); this means that the porosity of the beads is sufficient to minimize the resistance to intraparticle diffusion. Tanaka et al. (2013) reported different values for As(V) self-diffusivity in water; they proposed different values for self-diffusivity in function of As(V) speciation (Table AM6).

The variability in the two kinetic series is also demonstrated by the comparison of the equilibrium sorption capacities ($q_{eq,1}$) and apparent rate coefficients (i.e., k_1) for PFORE (and also PSORE). The apparent PFORE coefficient varies between 0.55 and 0.106 min^{-1} .

3.2.3. Sorption isotherms

The distribution of As(V) between solid and liquid phases at initial pH 7.1 (equilibrium pH ranging between 6.2 and 6.85) is represented by sorption isotherm (Fig. 2c). The model fits are calculated by combining the results of the two series. The lines show the fits of experimental profile with the three models (Langmuir, Sips and Freundlich) using the parameters reported in Table 3. The isotherm shows a progressive increase of the sorption capacity up to reaching a saturation plateau for an equilibrium concentration close to 5 mmol As g^{-1} . This asymptotic trend is not compatible with the power-type Freundlich equation. The Langmuir and the

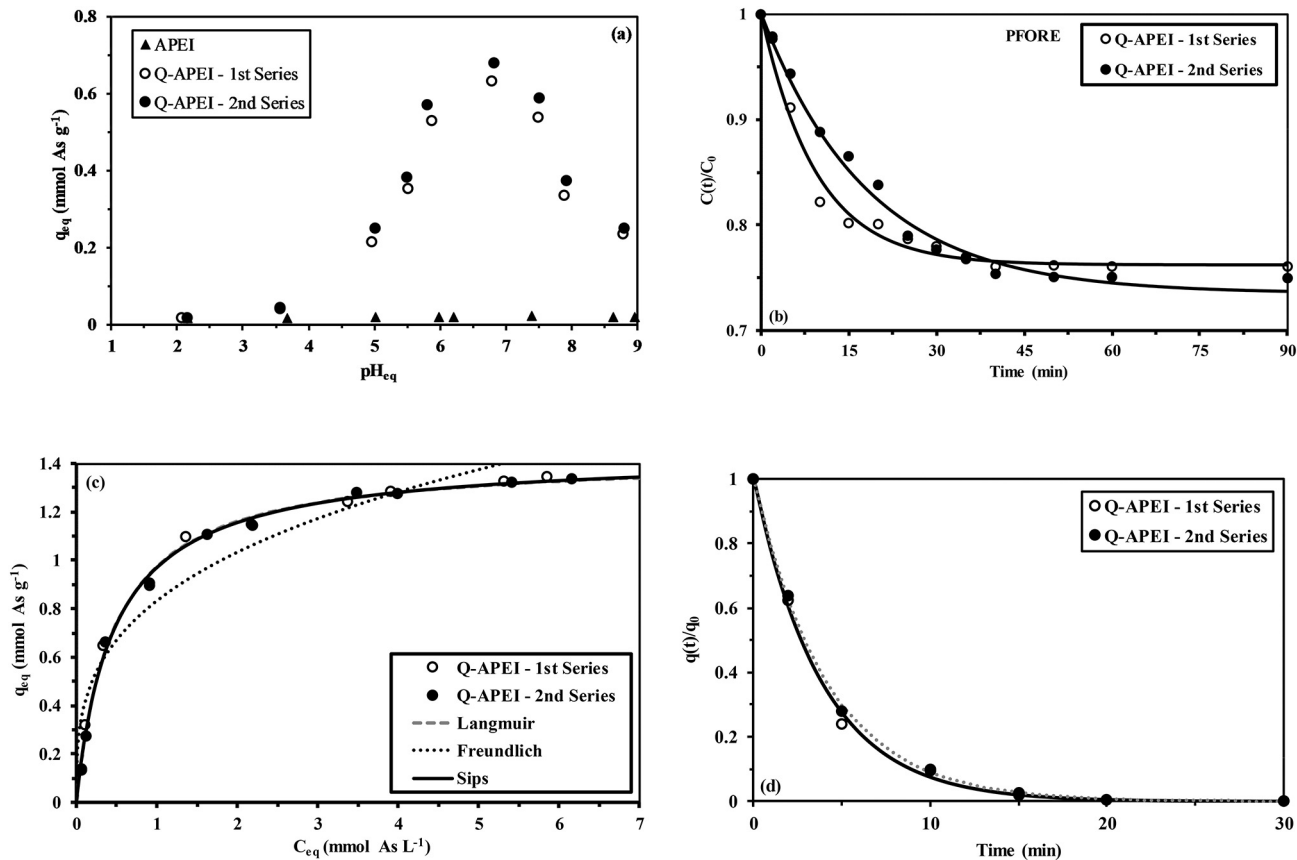


Fig. 2. a. pH effect on As(V) sorption using APEI* and Q-APEI* (C_0 : 0.645 mmol As L⁻¹ for APEI* and Q-APEI* – 1st Series, C_0 : 0.714 mmol As L⁻¹ for Q-APEI* – 2nd Series; sorbent dosage, SD: 1 g L⁻¹; time: 48 h; temperature, T: 22 (±2) °C; agitation speed: 165 (±5) rpm). b. As(V) uptake kinetics using APEI* and Q-APEI* – Modeling with the PFORE (C_0 : 0.65 mmol As L⁻¹ for Q-APEI* – 1st Series, C_0 : 0.71 mmol As L⁻¹ for Q-APEI* – 2nd Series; pH₀: 7.02–7.04; pH_{eq}: 6.75–6.79; SD: 0.25 g L⁻¹; temperature, T: 22 (±2) °C; agitation speed: 165 (±5) rpm). c. As (V) sorption isotherm using Q-APEI* sorbent at pH 7.1 (C_0 : 0.07–5.85 mmol As L⁻¹; time: 48 h; SD: 0.525 g L⁻¹; T: 22 (±2) °C; agitation speed: 165 (±5) rpm; pH_{eq}: 6.81–6.21). d. Desorption kinetics for As(V) loaded on Q-APEI* sorbent (sorbents collected from uptake kinetics (@ Fig. 3) (Eluent: 0.5 M CaCl₂/0.2 M HCl solution; SD: 1.25 g L⁻¹; T: 22 (±2) °C; agitation speed: 165 (±5) rpm).

Sips fits are overlapped; this is confirmed by the value of the equivalent-Freundlich coefficient in the equation (i.e., n_S), which is closed to 1. The maximum sorption capacity at saturation of the monolayer (i.e., $q_{m,L}$) tends to 1.43 mmol As g⁻¹, a little higher than the maximum experimental sorption capacity (i.e., 1.34 mmol As g⁻¹). This maximum sorption capacity can be compared with the nitrogen content of the Q-APEI* sorbent: 8 mmol N g⁻¹ (compared with 4.92 mmol N g⁻¹ for APEI*). The study of pH effect suggested a 1:1 stoichiometric exchange for the binding of H₂AsO₄⁻ on Q-APEI*. This means that all the amine groups are not available or accessible, including the proper quaternary ammonium groups (i.e., 3 mmol -N⁺). Hindrance effects, and/or the engagement of some reactive groups in secondary linkages may explain the

difference between theoretical stoichiometry and on the other side the effective relationship between the maximum sorption capacity and the number of reactive groups. The initial slope of the isotherm correlates to the affinity of the sorbent. Actually, Q-APEI* has a weak affinity for As(V): the 1 mmol As g⁻¹ sorption capacity requires a residual As(V) concentration in the solution around 1.1 mmol L⁻¹.

Table 4 compares the global sorption properties of different sorbents for As(V) (i.e., optimum pH, equilibrium time, and the Langmuir parameters for sorption isotherms). Some sorbents, such as functionalized resins (Chen et al., 2018; Lee et al., 2017; Zhang et al., 2018) or nano-structured materials (Azzam et al., 2017; Hokkanen et al., 2015) exhibit remarkable sorption properties ($q_{m,L}$: 2.46–5.75 mmol As g⁻¹).

Table 2
Parameters of models for As(V) uptake kinetics.

Model	Parameter	Fitted value – 1st Series	Fitted value – 2nd Series
Experimental	q_{eq} (mmol As g ⁻¹)	0.63	0.70
	$q_{eq,1}$ (mmol As g ⁻¹)	0.63	0.74
PFORE	k_1 (min ⁻¹)	0.11	0.055
	R^2	0.984	0.990
	$q_{eq,2}$ (mmol As g ⁻¹)	0.73	0.94
PSORE	k_2 (min ⁻¹)	0.17	0.058
	R^2	0.972	0.976
	$D_e \times 10^8$ (m ² min ⁻¹)	4.5	2.7
RIDE	R^2	0.949	0.971

D_0 (As(V)): 5.43×10^{-8} m² min⁻¹.

Table 3
Parameters of models for As(V) sorption isotherms.

Model	Parameter	Fitted value
Experimental	q_m (mmol As g ⁻¹)	1.34
	$q_{m,L}$ (mmol As g ⁻¹)	1.43
Langmuir	b_L (L mmol ⁻¹)	2.15
	R^2	0.994
	k_F	0.83
Freundlich	n_F	3.21
	R^2	0.927
	$q_{m,S}$ (mmol As g ⁻¹)	1.44
Sips	b_S (L mmol ⁻¹)	2.05
	n_S	1.03
	R^2	0.994

However, Q-APEI* shows a good compromise in terms of kinetics and saturation capacities, which are better than most of the alternative sorbents reported in recent literature.

Scheme 2 reports the different mechanisms that could be involved in As(V) sorption on the reactive groups present at the surface of Q-APEI* sorbent. Semi-quantitative EDX analysis, FTIR and XPS analyses, combined with the effect of pH (vs. pH_{PZC}) suggest that different mechanisms may take place in function of pH. The most probable mechanism consists of the anion-exchange of chloride ions with $H_2AsO_4^-$ in acidic conditions. This is consistent with the log plot of the distribution ratio vs. pH. XPS analysis confirms that a single As signal can be identified: a single type of interaction is involved in metalloid sequestration. When the pH increases (moderate alkaline solution) carboxylate groups of algal biomass and hydroxyl groups may interact with Na^+ and quaternary ammonium groups; this limits the availability and accessibility of reactive groups (quaternary ammonium). At higher pH (alkaline solution), the charge shielding with sodium cation (bound on negatively-charged carboxylate and hydroxyl groups) contributes to residual binding of another As(V) species, $HAsO_4^{2-}$.

3.2.4. Arsenic desorption and sorbent recycling

One of the most important challenge in the design of sorption process consists of the desorption of bound solute and the regeneration/recycling of the sorbent. The sensitivity of the sorbent to acid conditions (negligible sorption of As(V) in pH below 2) suggests using acidic solutions for releasing As(V) from loaded sorbent. The composition of the sorbent, made of alginate from algal biomass as the structuring support (in addition to functionalized PEI), may induce a certain sensitivity to the alternation of neutral and acidic conditions, in terms of sorbent stability. For this reason, in order to reinforce this stability, the acidic phase is completed with $CaCl_2$; which will contribute to the improvement of ionotropic gelation of carboxylic groups. Fig. 2d shows the desorption kinetics of As(V) using 0.5 M HCl/0.5 M $CaCl_2$ solution. The kinetic profiles for desorption were fitted with the equations reported in Table AM3; Table 5 summarizes the fitting parameters for the PFORE and PSORE for the desorption kinetics. Consistently with the uptake kinetics, the desorption kinetics profiles follow the PFORE model (superimposition of fitted curve and determination coefficient). It is noteworthy that the complete desorption of As(V) is obtained within 20 min. This means that desorption is faster than uptake, under selected experimental conditions. Table 6 compares the sorption and desorption

performances for five successive cycles. The sorption efficiency progressively decreases; however, even at the fifth cycle the sorption yield reaches 71% (compared with 81% at the first cycle). Under chosen conditions, the sorption capacity decreases from 0.681 mmol As g^{-1} to 0.601 mmol As g^{-1} . The desorption efficiency is even more stable: the decrease does not exceed 1.2% (from 99.7% to 98.5%) at the fifth cycle. This is consistent with the relative stability of the sorbent reported above in terms of surface characterization (FTIR). (See Table AM4.)

The combined sequence sorption/desorption allows concentrating metal ions (and As(V)). Arsenic can then be recovered by precipitation and more precisely co-precipitation with iron(III). At elevated concentrations of iron(III), adjustment of the pH causes metal precipitation, which is accompanied by the co-precipitation of other metal ions and compounds such as As(V) oxoanions (Cadena and Kirk, 1995; Robins et al., 2001; Senn et al., 2018). After solid/liquid (filtration, eventually assisted by coagulation/flocculation) the concentrated hazardous solid should be safely stored (Doerfelt et al., 2016), caring the storage conditions to prevent arsenic remobilization.

3.2.5. Treatment of acid mine drainage

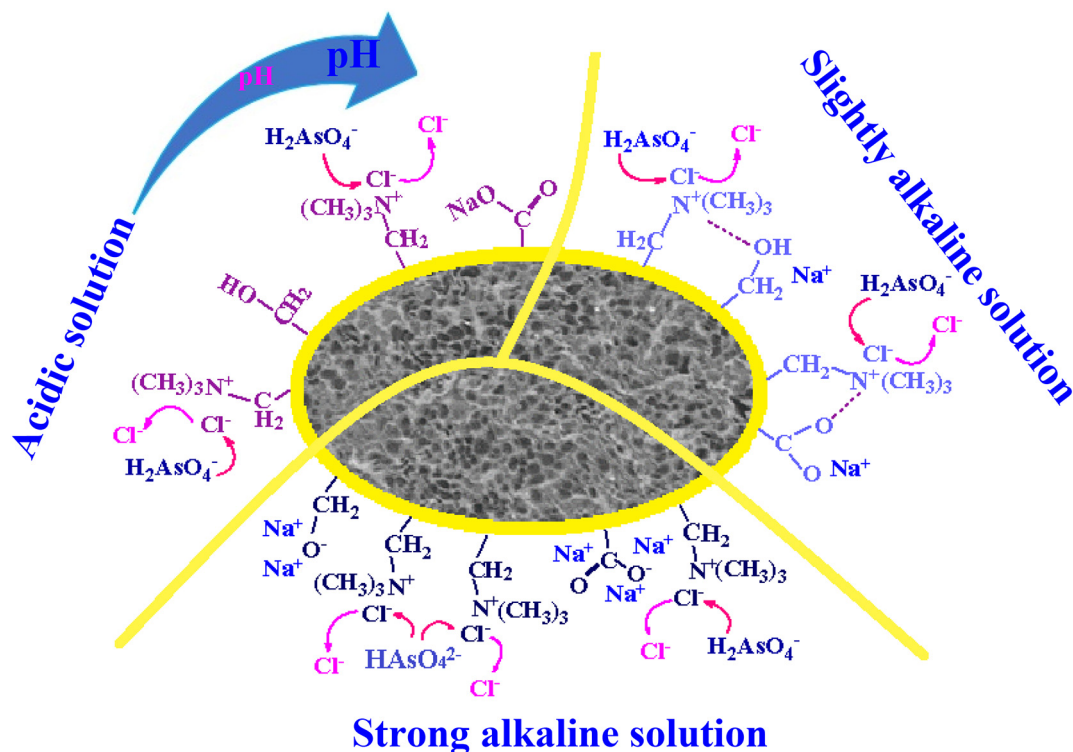
In order to evaluate the selectivity of the sorbent for As(V) but also to measure the potential of this material for practical application, Q-APEI* was also tested for the treatment of acid mine drainage (AMD, collected from an abandoned mining site located in Carnoulès, France). The study was focused on the impact of pH on the sorption of iron (predominant metal), zinc (tracer of heavy metals present in the local ore) and arsenic. The optimum pH for As(V) sorption on Q-APEI* being close to 7, the pH of acidic solutions was progressively increased. The pH increase causes the precipitation of some metals due to their high concentration in the water sample (especially iron). The precipitation of iron(III) hydroxide leads to the co-precipitation of As(V) and other metal ions. Therefore, the study examines first, the effect of pH control on the residual concentrations of As(V) and main metal ions in the filtrates, before studying more specifically the sorption of As(V) and metal ions from filtrated solutions.

3.2.5.1. Effect of pH control of metal and As(V) precipitation. The precipitation of iron and co-precipitation of other co-existing ions is reported in Figure AM12. The residual concentration of iron in the solution drastically decreases with rising the pH (from 23.3 mmol Fe L^{-1} down to 1.432 mmol Fe L^{-1}) at pH higher than 6 (abatement higher than 93%).

Table 4
Comparison of As(V) sorption on different sorbents.

Sorbent	pH	t_{eq}	$q_{m,L}$	b_L	Reference
Fe(III)-loaded resin	3.5	240	0.74	72	(Matsunaga et al., 1996)
Cu(OH) ₂ /Chitosan	4	1000	0.52	1.95	(Elwakeel and Guibal, 2015)
CuO/Chitosan	4	1000	0.38	2.70	(Elwakeel and Guibal, 2015)
Magnetic iron NPs/Cellulose	2	300	2.46	0.167	(Hokkanen et al., 2015)
Carbon foam	4.5	360	0.51×10^{-3}	2.88×10^6	(Agrawal et al., 2016)
Fe-loaded corn protein	6	960	0.026	3.75	(Thanawatpooontawee et al., 2016)
Fe ₃ O ₄ /bone char naocomposite	7	180	1.50×10^{-3}	2697	(Soltani et al., 2017)
Functionalized nanostructured composite	7	15	4.09	65.9	(Azzam et al., 2017)
Amine-doped acrylic fiber	3	30	2.67	95.9	(Lee et al., 2017)
Lewatit MP64	7.5	60	0.107	210	(Jose Alguacil and Escudero, 2018)
Quaternized polyphenylene sulfide resin	8-9	720	1.18	-	(Shao et al., 2017)
Diethylenetriamine functionalized resin	4	120	5.25	73.45	(Zhang et al., 2018)
Polyamine chelating hyperbranched resin	4	360	5.75	5819	(Chen et al., 2018)
S-doped Fe ₃ O ₄ NPs	6	240	0.78	72.7	(Liu et al., 2018)
MOF (Zr- UiO-66)	2	30	1.15	24.8	(Shahat et al., 2018)
Functionalized MOF	7	180	1.90	106	(Awual et al., 2019)
Crown ether/Fe/Amberlite XAD7	7-8	300	0.391	1349	(Ciopec et al., 2019)
Fe-Mn/Clay	4	60	1.61	3.22	(Foroutan et al., 2019)
Al-impregnated biochar	7.6	300	0.035	608	(Liu et al., 2019)
Fe(NO ₃) ₃ /Graphene	7	60	1.50	107	(Qu et al., 2019)
ZrO/SiO ₂	6.5	2880	1.2	-	(Hocaoglu et al., 2019)
Algal-based biochar	4	30	0.102	170	(Senthilkumar et al., 2020)
Q-APEI*	7	45	1.43	2.15	This study

t_{eq} (equilibrium time, min), $q_{m,L}$ (mmol As g^{-1}); b_L (L mmol⁻¹).



Scheme 2. Tentative mechanisms for As(V) sorption on specific reactive groups held on Q-APEI*.

Arsenic concentration progressively decreases from 2.669 mmol As L⁻¹ to 1.295 mmol L⁻¹ at pH 6.3: while increasing the pH above 6.3 the concentration of As(V) stabilizes to 1.094 mmol As L⁻¹. The initial concentration of Zn is close to 0.306 mmol Zn L⁻¹; a slight decrease (<15%) is observed up to pH 6.3. Above pH 6.3, concentration decreased by the effect of dilution during pH adjustment (up to 40%) but stabilizes at pH 7: residual concentration stabilizes around 0.176 mmol Zn L⁻¹. This is confirmed by the EDX analysis of the precipitate cakes (Figure AM13): coprecipitation concerns Al, Si, S, Ca, Fe (50–79% of weight percentage), and As elements.

3.2.5.2. Effect of pH on metal and As(V) removal. Fig. 3 shows the increase of the sorption capacities for As(V), Zn(II) and Fe with pH (including the cumulative sorption capacity) for a contact time of 20 h. Other contact times are reported in Figure AM14: a significant increase is observed by increasing the contact time from 8 h to 20 h; for longer contact times, the enhancement of sorption capacities is minimized. The maximum sorption capacities are reached at pH 7.23 for Zn(II) (i.e., 0.52 mmol Zn g⁻¹), and As(V) (i.e., 0.73 mmol As g⁻¹), and pH 7.83 for Fe (i.e., 0.94 mmol Fe g⁻¹). The cumulative sorption capacity reaches 2.12 mmol metal g⁻¹ at pH 7.83.

For the AMD controlled at pH 6.33 (which corresponds to approximately the pH reached in the sorption isotherm), the residual concentration reaches 1.07 mmol As g⁻¹ and the sorption capacity is close to 0.67 mmol As g⁻¹. For this residual concentration, the sorption capacity reaches about 1 mmol As g⁻¹ in the synthetic pure solutions (Fig. 3). This means that the presence of co-existing ions reduces by one third

the sorption capacity of Q-APEI* for As(V). The cumulative sorption capacity tends to 1.52 mmol metal g⁻¹. This means that the other metals may compete for the same reactive groups but also some other reactive groups may be involved in the binding of competitor ions; for example on hydroxyls and carboxylate groups, which have high affinity for heavy metals. Figure AM15 compares the EDX analyses of the surface of Q-APEI* after being equilibrated with pH-controlled AMD samples. The surface porous structure does not appear to be changed by the pH and by the binding of the different elements.

Figure AM16 compares the effect of pH, at different contact times, on the selectivity coefficient (SC, dimensionless) of As against Zn and Fe;

$$\text{Selectivity coefficient } SC = \frac{D_{As}}{D_{metal}} = \frac{q_{eq}(As) \times C_{eq}(metal)}{C_{eq}}(As) \times q_{eq}(metal) \quad (1)$$

The selectivity for As(V) strongly depends on the pH and the metal. The selectivity coefficient of Q-APEI* for As/Fe drastically decreases (from 22 to 1.4) with increasing the pH (in the range 1.54–4.94); above pH 6.33, the SC stabilizes around 0.7. A reciprocal trend is obtained for the system As/Zn; indeed, the sorbent is selective for Zn over As, especially above pH 6.33 (SC varies between 58 and 123). The sorbent cannot be considered selective for As(V) and the experimental conditions should take into account the sorption capacities rather than the eventual selectivity.

3.2.5.3. Effect of sorbent dosage on metal and As(V) removal. Fig. 4 shows the effect of sorbent dosage on the sorption capacity and sorption efficiency for the different selected contaminants. As expected, increasing sorbent dosage enhances the removal efficiency: total recovery of zinc is observed at a sorbent dosage of 1 g L⁻¹ (lower initial concentration of Zn). Sorbent dosage must be increased to 2 g L⁻¹ for achieving the complete uptake of As(V) while total extraction of Fe requires a higher dosage (close to 3 g L⁻¹).

Table 5
Modeling of kinetic profiles for As(V) desorption from loaded Q-APEI* sorbent – PFORE and PSORE model (Lazaridis et al., 2004).

Sorbent	Model Parameter	PFORE		PSORE		
		k _{d1} (min ⁻¹)	R ²	β ₂	k _{d2} (min ⁻¹)	R ²
Q-APEI* 1st		0.26	0.998	0.98	0.51	0.974
Q-APEI* 2nd		0.24	0.999	0.98	0.47	0.972

Table 6

As(V) desorption and sorbent recycling.

Cycle #	Sorption efficiency (%)		Desorption efficiency (%)	
	Average	S.D.	Average	S.D.
1	81.7	0.8	99.7	0.5
2	80.2	1.0	99.1	0.6
3	77.5	1.5	98.3	1.7
4	74.6	1.4	98.8	0.7
5	71.6	1.6	98.5	0.5

(Experimental conditions – Sorption: C_0 : 54 mg As L⁻¹ = 0.72 mmol As L⁻¹; pH: 7.0; SD: 0.89 g L⁻¹; time: 24 h; T: 22(±2); agitation speed: 165 (±5) rpm/Desorption: eluent: 0.5 M CaCl₂/0.2 M HCl; SD: 3.3 g L⁻¹; time: 2 h; T: 22(±2) °C; agitation speed: 165 (±5) rpm).

Logically, the sorption capacity decreases with sorbent dosage for Zn (II); the variations are less marked for As(V) and Fe (cumulative sorption capacity decreases from 1.69 to 0.99 mmol metal g⁻¹). A sorbent dosage of 3 g L⁻¹ is sufficient for achieving the decontamination of the AMD at pH 7, with sorption capacities close to 0.43 mmol As g⁻¹, 0.48 mmol Fe g⁻¹ and 0.086 mmol Zn g⁻¹.

Q-APEI* can be considered a promising polishing treatment after pH control to 7, providing a sorbent dosage close to 3 g L⁻¹.

4. Conclusion

The composite material based on the interaction of *Laminaria digitata* biomass with PEI (under controlled conditions of pH, pre-extraction of alginate and crosslinking with glutaraldehyde) is successfully quaternized (synthesis of Q-APEI*). This chemical modification strongly increases the sorption properties of the composite material for As(V). Under the most favorable conditions (i.e., at pH close to 6.5–7), the sorption of As(V) proceeds through ion-exchange mechanism between H₂AsO₄⁻ and chloride anions on quaternary ammonium salt. The porous beads allow relatively fast kinetics: under selected experimental conditions, equilibrium is achieved within 40 min. The sorption isotherm is fitted by the Langmuir equation: maximum sorption capacity reaches 1.34 mmol As g⁻¹, though the affinity coefficient is relatively weak (i.e., 2.15 mmol L⁻¹). Arsenic can be readily desorbed from loaded sorbent using an acidic calcium chloride solution: desorption kinetics is even faster than uptake kinetics and the sorbent can be recycled for 5 cycles with a limited decrease in sorption efficiency and good stability in terms of desorption efficiency (higher than 98%). The sorbent reveals highly efficient for As(V) sorption from complex acid mine

drainage solutions (after pH control). After this precipitation pretreatment, Q-APEI* can be used as a polishing step for removing As (V) and other residual metal ions. In this complex effluent, the sorption capacity reaches up to 0.76 mmol As g⁻¹, despite the presence of high concentrations of co-existing ions. This new sorbent reveals very promising as a polishing treatment or for the primary treatment of As (V) effluents (at mild concentrations, lower than 100 mg As L⁻¹, containing mild concentrations of co-ions).

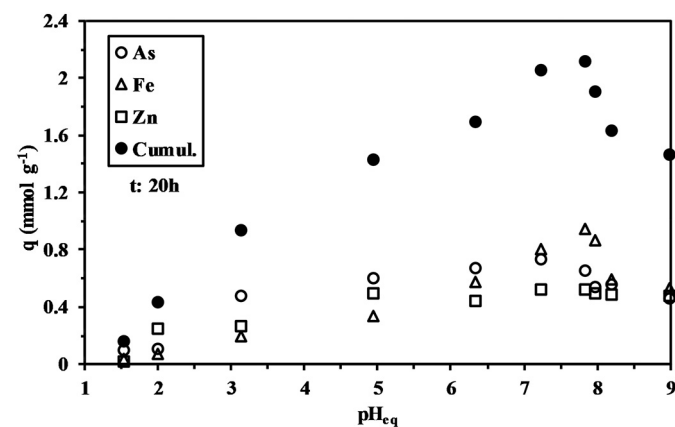


Fig. 3. Effect of pH on the recovery of As, Fe and Zn (and cumulative sorption capacity) using Q-APEI* (contact time: 20 h; SD: 0.33 g L⁻¹; T: 22 (±2) °C; agitation speed: 165 (±5) rpm).

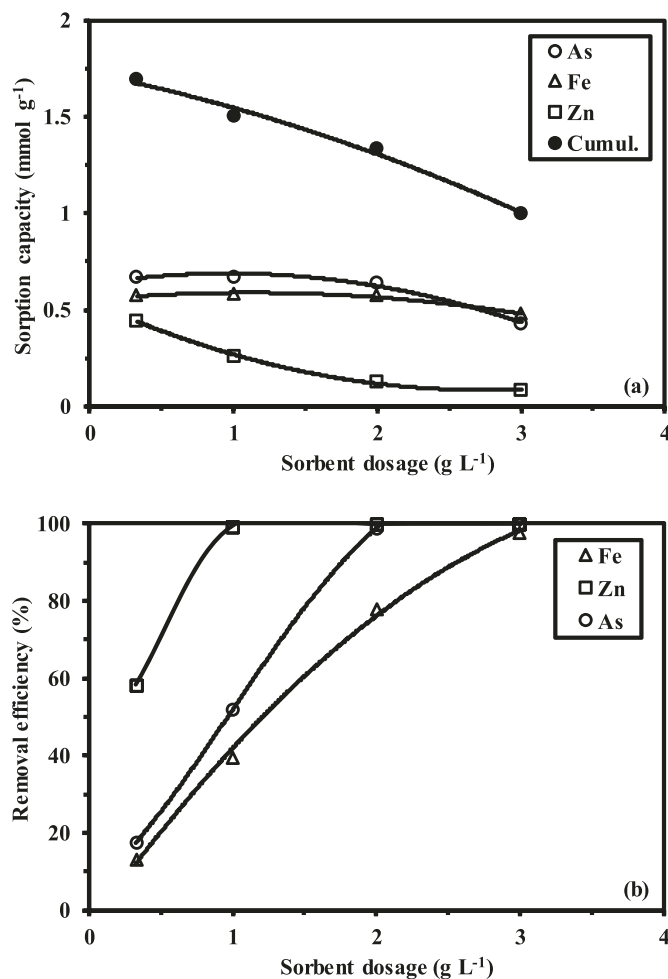


Fig. 4. Effect of sorbent dosage on (a) the sorption capacity and (b) the removal efficiency of As, Fe and Zn (and cumulative sorption capacity) using Q-APEI* (SD: 0.33–3 g L⁻¹; contact time: 20 h; pH₀: 5; pH_{eq}: 6.3–5.9; T: 22 (±2) °C; agitation speed: 165 (±5) rpm).

CRedit authorship contribution statement

Mohammed F. Hamza: Conceptualization, Methodology, Resources, Data curation, Supervision, Writing - original draft, Writing - review & editing. **Siming Lu:** Investigation. **Khalid A.M. Salih:** Investigation. **Hamed Mira:** Resources. **Abdelghaffar S. Dhmees:** Formal analysis. **Toyohisa Fujita:** Project administration. **Yuezhou Wei:** Conceptualization, Methodology, Supervision, Project administration. **Thierry Vincent:** Resources, Data curation. **Eric Guibal:** Conceptualization, Methodology, Resources, Writing - original draft, Writing - review & editing.

Declaration of competing interest

The authors declare that they have no known competing financial interests or personal relationships that could have appeared to influence the work reported in this paper.

Acknowledgements

Eric Guibal and Mohammed F Hamza acknowledge the support of the IMHOTEP Program (MetalValor project) from French Government (Institut Français d'Egypte) and Egyptian Academy of Science & Technology (Science and Technology Development Fund). Yuezhou Wei thanks the support of NSFC Projects (No.11675102, No.11975082, U1967218). Shengye Wang and Yayuan MO (IMT-Mines Ales) are acknowledged for their technical assistance in synthesizing APEI* beads.

Appendix A. Supplementary data

Supplementary data to this article can be found online at <https://doi.org/10.1016/j.scitotenv.2020.137396>.

References

Agrawal, P.R., Kumar, R., Uppal, H., Singh, N., Kumari, S., Dhakate, S.R., 2016. Novel 3D lightweight carbon foam as an effective adsorbent for arsenic(V) removal from contaminated water. *RSC Adv.* 6, 29899–29908.

Asere, T.G., Stevens, C.V., Du Laing, G., 2019. Use of (modified) natural adsorbents for arsenic remediation: a review. *Sci. Total Environ.* 676, 706–720.

Awual, M.R., Hasan, M.M., Asiri, A.M., Rahman, M.M., 2019. Cleaning the arsenic (V) contaminated water for safe-guarding the public health using novel composite material. *Composites Part B-Engineering* 171, 294–301.

Azzam, A.M., Shenashen, M.A., Selim, M.M., Yamaguchi, H., El-Sewify, I.M., Kawada, S., et al., 2017. Nanospherical inorganic alpha-Fe core-organic shell necklaces for the removal of arsenic(V) and chromium(VI) from aqueous solution. *J. Phys. Chem. Solids* 109, 78–88.

Barakan, S., Aghazadeh, V., 2019. Structural modification of nano bentonite by aluminum, iron pillarization and 3D growth of silica mesoporous framework for arsenic removal from gold mine wastewater. *J. Hazard. Mater.* 378.

Cadena, F., Kirk, T.L., 1995. Arsenate Precipitation Using Ferric Iron in Acidic Conditions. USDOE, Washington, DC, USA Washington, DC (United States); Amoco Production Co., Houston, TX (United States); Conoco, Inc., Stamford, CT (United States).

Chaudhry, S.A., Khan, T.A., Ali, I., 2017. Zirconium oxide-coated sand based batch and column adsorptive removal of arsenic from water: isotherm, kinetic and thermodynamic studies. *Egypt. J. Petrol.* 26, 553–563.

Chen, Y.N., Zhao, W., Wang, H., Li, Y.H., Li, C.X., 2018. Preparation of novel polyamine-type chelating resin with hyperbranched structures and its adsorption performance. *R. Soc. Open Sci.* 5, 15.

Ciopec, M., Negrea, A., Lupa, L., Davidescu, C.M., Negrea, P., 2014. Studies regarding As (V) adsorption from underground water by Fe-XAD8-DEHPA impregnated resin. Equilibrium sorption and fixed-bed column tests. *Molecules* 19, 16082–16101.

Ciopec, M., Davidescu, C.M., Negrea, A., Duteanu, N., Rusu, G., Grad, O., et al., 2019. Amberlite XAD7 resin functionalized with crown ether and Fe(III) used for arsenic removal from water. *Pure Appl. Chem.* 91, 375–388.

Crank, J., 1975. *The Mathematics of Diffusion*. Oxford University Press, Oxford, U.K.

Dambies, L., Vincent, T., Guibal, E., 2002. Treatment of arsenic-containing solutions using chitosan derivatives: uptake mechanism and sorption performances. *Water Res.* 36, 3699–3710.

Deliyanni, E.A., Kyzas, G.Z., Triantafyllidis, K.S., Matis, K.A., 2015. Activated carbons for the removal of heavy metal ions: a systematic review of recent literature focused on lead and arsenic ions. *Open Chemistry* 13, 699–708.

Doerfelt, C., Feldmann, T., Roy, R., Demopoulos, G.P., 2016. Stability of arsenate-bearing Fe (III)/Al(III) co-precipitates in the presence of sulfide as reducing agent under anoxic conditions. *Chemosphere* 151, 318–323.

Dong, F., Xu, X., Shaghaleh, H., Guo, J., Guo, L., Qian, Y., et al., 2019. Factors influencing the morphology and adsorption performance of cellulose nanocrystal/iron oxide nanorod composites for the removal of arsenic during water treatment. *Int. J. Biol. Macromol.* <https://doi.org/10.1016/j.ijbiomac.2019.11.182> in press.

Dos Santos Araujo, P., Belini, G.B., Mambrini, G.P., Yamaji, F.M., Waldman, W.R., 2019. Thermal degradation of calcium and sodium alginate: a greener synthesis towards calcium oxide micro/nanoparticles. *Int. J. Biol. Macromol.* 140, 749–760.

Drahota, P., Filipi, M., Ettler, V., Rohovec, J., Mihaljevic, M., Sebek, O., 2012. Natural attenuation of arsenic in soils near a highly contaminated historical mine waste dump. *Sci. Total Environ.* 414, 546–555.

Elwakeel, K.Z., Guibal, E., 2015. Arsenic(V) sorption using chitosan/cu(OH)₂ and chitosan/CuO composite sorbents. *Carbohydr. Polym.* 134, 190–204.

Farasin, J., Andres, J., Casiot, C., Barbe, V., Faerber, J., Halter, D., et al., 2015. *Thiomonas* sp CB2 is able to degrade urea and promote toxic metal precipitation in acid mine drainage waters supplemented with urea. *Front. Microbiol.* 6, 15.

Foroutan, R., Mohammadi, R., Adeleye, A.S., Farjadfar, S., Esvandi, Z., Arfaeina, H., et al., 2019. Efficient arsenic(V) removal from contaminated water using natural clay and clay composite adsorbents. *Environ. Sci. Pollut. Res. Int.* <https://doi.org/10.1007/s11356-019-06070-5> press.

Halder, D., Biswas, A., Slejkovec, Z., Chatterjee, D., Nriagu, J., Jacks, G., et al., 2014. Arsenic species in raw and cooked rice: implications for human health in rural Bengal. *Sci. Total Environ.* 497, 200–208.

Hamza, M.F., Wei, Y., Guibal, E., 2020. Quaternization of algal/PEI beads (a new sorbent): characterization and application to scandium recovery from aqueous solutions. *Chem. Eng. J.* <https://doi.org/10.1016/j.cej.2019.123210> (in press).

Haron, M.J., Yunus, W., Yong, N.L., Tokunaga, S., 1999. Sorption of arsenate and arsenite anions by iron(III)-poly(hydroxamic acid) complex. *Chemosphere* 39, 2459–2466.

He, J., Ni, F., Cui, A., Chen, X., Deng, S., Shen, F., et al., 2020. New insight into adsorption and co-adsorption of arsenic and tetracycline using a Y-immobilized graphene oxide-alginate hydrogel: adsorption behaviours and mechanisms. *Sci. Total Environ.* 701, 134363.

Ho, Y.S., McKay, G., 1999. Pseudo-second order model for sorption processes. *Process Biochem.* 34, 451–465.

Hocaoğlu, S.M., Wakui, Y., Suzuki, T.M., 2019. Separation of arsenic(V) by composite adsorbents of metal oxide nanoparticles immobilized on silica flakes and use of adsorbent coated alumina tubes as an alternative method. *Journal of Water Process Engineering* 27, 134–142.

Hokkanen, S., Repo, E., Lou, S., Sillanpää, M., 2015. Removal of arsenic(V) by magnetic nanoparticle activated microfibrillated cellulose. *Chem. Eng. J.* 260, 886–894.

Jeong H, Kim H, Jang T. Irrigation water quality standards for indirect wastewater reuse in agriculture: a contribution toward sustainable wastewater reuse in South Korea. *Water* 2016; 8: art. 169.

Jose Alguacil, F., Escudero, E., 2018. Removal of arsenic(V) from aqueous wastes by ion exchange with Lewatit MP64 resin. *Desalin. Water Treat.* 133, 257–261.

Kumar, I., Quaff, A.R., 2019. Comparative study on the effectiveness of natural coagulant aids and commercial coagulant: removal of arsenic from water. *Int. J. Environ. Sci. Technol.* 16, 5989–5994.

Lazaridis, N.K., Pandi, T.A., Matis, K.A., 2004. Chromium(VI) removal from aqueous solutions by Mg-Al-CO₃ hydrotalcite: sorption-desorption kinetic and equilibrium studies. *Ind. Eng. Chem. Res.* 43, 2209–2215.

Lee, C.-G., Alvarez, P.J.J., Nam, A., Park, S.-J., Do, T., Choi, U.-S., et al., 2017. Arsenic (V) removal using an amine-doped acrylic ion exchange fiber: kinetic, equilibrium, and regeneration studies. *J. Hazard. Mater.* 325, 223–229.

Li, T., Zhang, Y., Zhang, B., Chang, K., Jiao, F., Qin, W., 2019. Arsenic(V) removal from enargite leach solutions by precipitation of magnesium ammonium arsenate. *Sep. Sci. Technol.* 54, 1862–1870.

Liu, M., Sun, Y., Na, S., Yan, F., 2016. Selective adsorption of lead(II) from aqueous solution by ion-imprinted PEI-functionalized silica sorbent: studies on equilibrium isotherm, kinetics, and thermodynamics. *Desalin. Water Treat.* 57, 3270–3282.

Liu, J., Kong, L., Huang, X., Liu, M., Li, L., 2018. Removal of arsenic(v) from aqueous solutions using sulfur-doped Fe₃O₄ nanoparticles. *RSC Adv.* 8, 40804–40812.

Liu, Q., Wu, L., Gorrng, M., Deng, Y., 2019. Aluminum-impregnated biochar for adsorption of arsenic(V) in urban stormwater runoff. *J. Environ. Eng.* 145.

Lu, S., Chen, L., Hamza, M.F., He, C., Wang, X., Wei, Y., et al., 2019. Amidoxime functionalization of a poly(acrylonitrile)/silica composite for the sorption of Ga(III) – application to the treatment of Bayer liquor. *Chem. Eng. J.* 368, 459–473.

Marcus, Y., 1997. *Ion Properties*. Marcel Dekker, Inc, New York, NY.

Matsunaga, H., Yokoyama, T., Eldridge, R.J., Bolto, B.A., 1996. Adsorption characteristics of arsenic(III) and arsenic(V) on iron(III)-loaded chelating resin having lysine-N-alpha, N-alpha-diacetic acid moiety. *Reactive & Functional Polymers* 29, 167–174.

Membre, E., Sails, P., 2018. Thermochemical characterization of brown seaweed, *Laminaria digitata* from UK shores. *J. Anal. Appl. Pyrolysis* 131, 42–51.

Miller, J.R., Hudson-Edwards, K.A., Lechler, P.J., Preston, D., Macklin, M.G., 2004. Heavy metal contamination of water, soil and produce within riverine communities of the Rio Pilcomayo basin, Bolivia. *Sci. Total Environ.* 320, 189–209.

Ng, J.C., Wang, J.P., Shraim, A., 2003. A global health problem caused by arsenic from natural sources. *Chemosphere* 52, 1353–1359.

Niazi, N.K., Bibi, I., Shahid, M., Ok, Y.S., Shaheen, S.M., Rinklebe, J., et al., 2018. Arsenic removal by Japanese oak wood biochar in aqueous solutions and well water: investigating arsenic fate using integrated spectroscopic and microscopic techniques. *Sci. Total Environ.* 621, 1642–1651.

Oehmen, A., Valerio, R., Llanos, J., Fradinho, J., Serra, S., Reis, M.A.M., et al., 2011. Arsenic removal from drinking water through a hybrid ion exchange membrane – coagulation process. *Sep. Purif. Technol.* 83, 137–143.

Padungthong, S., German, M., Wiriyathamcharoen, S., SenGupta, A.K., 2015. Polymeric anion exchanger supported hydrated Zr(IV) oxide nanoparticles: a reusable hybrid sorbent for selective trace arsenic removal. *React. Funct. Polym.* 93, 84–94.

Phan, K., Shthianopkka, S., Kim, K.-W., Wong, M.H., Sao, V., Hashim, J.H., et al., 2010. Health risk assessment of inorganic arsenic intake of Cambodia residents through groundwater drinking pathway. *Water Res.* 44, 5777–5788.

- Qu, G., Li, R., Zhou, Y., Wu, B., Cai, Y., Ning, P., 2019. Preparation of ferric nitrate-graphene nanocomposite and its adsorption of arsenic(V) from simulated arsenic-containing wastewater. *Appl. Organomet. Chem.* <https://doi.org/10.1002/aoc.5221> in press.
- Robins, R.G., Nishimura, T., Singh, P., 2001. Removal of arsenic from drinking water by precipitation, adsorption or cementation. In: Feroze, A., Ashraf Ali, M., Adeel, Z. (Eds.), *Technologies for Arsenic Removal from Drinking Water*. Bangladesh University of Engineering and Technology and the United Nations University, Dhaka, Bangladesh, pp. 31–42.
- Sahiner, N., Demirci, S., Sahiner, M., Al-Lohedan, H., 2015. The synthesis of desired functional groups on PEI microgel particles for biomedical and environmental applications. *Appl. Surf. Sci.* 354, 380–387.
- Senn, A.-C., Hug, S.J., Kaegi, R., Hering, J.G., Voegelin, A., 2018. Arsenate co-precipitation with Fe(II) oxidation products and retention or release during precipitate aging. *Water Res.* 131, 334–345.
- Senthilkumar, R., Prasad, D.M.R., Govindarajan, L., Saravanakumar, K., Prasad, B.S.N., 2020. Synthesis of green marine algal-based biochar for remediation of arsenic(V) from contaminated waters in batch and column mode of operation. *Int. J. Phytorem.* 22 (3), 279–286.
- Shahat, A., Hassan, H.M.A., Azzazy, H.M.E., Hosni, M., Awual, M.R., 2018. Novel nano-conjugate materials for effective arsenic(V) and phosphate capturing in aqueous media. *Chem. Eng. J.* 331, 54–63.
- Shakoor, M.B., Niazi, N.K., Bibi, I., Shahid, M., Sharif, F., Bashir, S., et al., 2018. Arsenic removal by natural and chemically modified water melon rind in aqueous solutions and groundwater. *Sci. Total Environ.* 645, 1444–1455.
- Shao, G., Yao, H., Liu, A., Zhang, Z., Huang, J., Yuan, S., 2017. Polyphenylene sulfide-based adsorption resins: synthesis, characterization and adsorption performance for Hg(II) and As(V). *Polym. Adv. Technol.* 28, 1735–1742.
- Sigrist, M.E., Beldomenico, H.R., Tarifa, E.E., Pieck, C.L., Vera, C.R., 2011. Modelling diffusion and adsorption of As species in Fe/GAC adsorbent beds. *J. Chem. Technol. Biotechnol.* 86, 1256–1264.
- Soltani, R.D.C., Safari, M., Maleki, A., Rezaee, R., Shahmoradi, B., Shahmohammadi, S., et al., 2017. Decontamination of arsenic(V)-contained liquid phase utilizing Fe₃O₄/bone char nanocomposite encapsulated in chitosan biopolymer. *Environ. Sci. Pollut. Res.* 24, 15157–15166.
- Tanaka, M., Takahashi, Y., Yamaguchi, N., Kim, K.-W., Zheng, G., Sakamitsu, M., 2013. The difference of diffusion coefficients in water for arsenic compounds at various pH and its dominant factors implied by molecular simulations. *Geochim. Cosmochim. Acta* 105, 360–371.
- Thanawatpooantawee, S., Imyim, A., Praphairaksit, N., 2016. Iron-loaded zein beads as a biocompatible adsorbent for arsenic(V) removal. *J. Ind. Eng. Chem.* 43, 127–132.
- Thi Hanh, N., Thi Huong, P., Hong Tham Nguyen, T., Thi Nham, N., Minh-Viet, N., Trinh Tran, D., et al., 2019. Synthesis of iron-modified biochar derived from rice straw and its application to arsenic removal. *Journal of Chemistry* 2019.
- Tien, C., 1994. *Adsorption Calculations and Modeling*. Butterworth-Heinemann, Newton, MA.
- Tiwari, D., Lee, S.M., 2012. Novel hybrid materials in the remediation of ground waters contaminated with As(III) and As(V). *Chem. Eng. J.* 204, 23–31.
- Tuchowska, M., Wolowicz, M., Solinska, A., Koscielniak, A., Bajda, T., 2019. Organomodified vermiculite: preparation, characterization, and sorption of arsenic compounds. *Minerals* 9.
- USEPA (Ed.), 2012. *The Drinking Water Standards and Health Advisories*. USEPA, Washington, DC, pp. 1–12 822-S-12-001.
- Wang, S., Vincent, T., Faur, C., Guibal, E., 2018. A comparison of palladium sorption using polyethyleneimine impregnated alginate-based and carrageenan-based algal beads. *Applied Sciences-Basel* 8.
- Wang, S., Vincent, T., Faur, C., Rodriguez-Castellon, E., Guibal, E., 2019. A new method for incorporating polyethyleneimine (PEI) in algal beads: high stability as sorbent for palladium recovery and supported catalyst for nitrophenol hydrogenation. *Mater. Chem. Phys.* 221, 144–155.
- Wei Y, Salih KAM, Lu S, Hamza MF, Fujita T, Vincent T, et al. Amidoxime functionalization of algal/polyethyleneimine beads for the sorption of Sr(II) from aqueous solutions. *Molecules* 2019a; 24: Art. N° 3893.
- Wei, Y., Wei, S., Liu, C., Chen, T., Tang, Y., Ma, J., et al., 2019b. Efficient removal of arsenic from groundwater using iron oxide nanoneedle array-decorated biochar fibers with high Fe utilization and fast adsorption kinetics. *Water Res.* 167.
- Xiao, Y.F., Huang, W.J., Xu, K.J., Li, M.X., Fan, M.M., Wang, K., 2018. Preparation of anion exchange membrane with branch polyethyleneimine as main skeleton component. *Mater. Des.* 160, 698–707.
- Yan, X., Fei, Y., Zhong, L., Wei, W., 2019. Arsenic stabilization performance of a novel starch-modified Fe-Mn binary oxide colloid. *Sci. Total Environ.* 136064.
- Yin, Z., Luetzenkirchen, J., Finck, N., Celaries, N., Dardenne, K., Hansen, H.C.B., 2019. Adsorption of arsenic(V) onto single sheet iron oxide: X-ray absorption fine structure and surface complexation. *J. Colloid Interface Sci.* 554, 433–443.
- Yousif, A.M., Zaid, O.F., Ibrahim, I.A., 2016. Fast and selective adsorption of As(V) on prepared modified cellulose containing Cu(II) moieties. *Arab. J. Chem.* 9, 607–615.
- Zacarias-Estrada, O.L., Ballinas-Casarrubias, L., Montero-Cabrera, M.E., Loredó-Portales, R., Orrantia-Borunda, E., Luna-Velasco, A., 2019. Arsenic removal and activity of a sulfate reducing bacteria-enriched anaerobic sludge using zero valent iron as electron donor. *J. Hazard. Mater.* 384, 121392. <https://doi.org/10.1016/j.jhazmat.2019.121392>.
- Zhang, J.C., Chen, Y.N., Zhao, W., Li, Y.H., 2018. Arsenic removal from aqueous solutions by diethylenetriamine-functionalized resin: isotherm, kinetics, selectivity and mechanism. *R. Soc. Open Sci.* 5, 10.